Direct Three-Dimensional Patterson Inversion of Low-Energy Electron Diffraction $I(E)$ Curves

C. Y. Chang,[1] Z. C. Lin,[1] Y. C. Chou,[1] and C. M. Wei[2]
[1]*Department of Physics, National Tsing-Hua University, Hsin-Chu, Taiwan 30055, Republic of China*
[2]*Institute of Physics, Academia Sinica, Nan-Kang, Taipei, Taiwan 11529, Republic of China*
(Received 22 April 1999)

A Patterson-like scheme is proposed for direct inversion of the conventional low-energy electron diffraction (LEED) intensity versus energy $I(E)$ curves, which is in contrast with the previously suggested holographic scheme. Using the Si(111)-(7 × 7) and Si(113)-(3 × 2) surfaces as examples, high quality three-dimensional images, with a resolution better than 0.5 Å, of both surface atoms and bulk atoms are obtained from the direct Patterson inversion of LEED-$I(E)$ curves with the integral-energy phase-summing method.

PACS numbers: 61.14.Hg, 61.14.Nm, 61.18.–j

The determination of surface structure is the first step for thorough understanding of surface properties. Many surface structural techniques need an approximate structure model as an input for the refinement calculation. The dynamical low-energy electron diffraction (LEED) calculation is one example. When the surfaces are prepared, the surfaces can either relax or reconstruct to lower their surface energy. In the case of surface reconstruction, the unit cell of the surface is larger than that of the bulk. The Si(111)-(7 × 7) and Si(113)-(3 × 2) surfaces are good examples (abbreviated as 7 × 7 and 3 × 2 thereafter). However, a general rule to determine the approximate model of a large surface unit cell did not exist. It is a long-term goal for the surface structure technique to search direct methods to image the three dimensional (3D) atomic images of the surface region. In the early stage of development of LEED, efforts have been made to extract surface structural information by direct inversion of LEED intensity versus incident energy $[I(E)]$ curves [1,2], and by the constant-momemtum-transfer-averaging analysis of the LEED intensities [3]. However, only limited progress has been made. After the initialization of the notion of electron emission holography [4–6], the holographic idea was applied to LEED-$I(E)$ curves of surface with adsorbed atoms [7–10]. The feasibility of holographic inversion of LEED-$I(E)$ curves of a more general surface is still unclear.

In the holographic idea, the reference wave can be identified as the scattered wave resulting from the first scattering process from a surface atom (emitter). The object wave is the subsequently diffracted wave of the reference wave scattered by a nearby atom (scatterer). The interference between the reference wave and the object wave results in a hologram of the surface atomic pair. Thus the holographic process is intrinsically a multiple scattering process; see Fig. 1(a). As for LEED, in which only the elastic scattering is involved, the holographic process constitutes just a portion of electron-matter interaction. Another major part of the scattering process depicted in Fig. 1(b) is the single scattering process, which has long been adopted to get the Patterson function of the bulk sample by inverting the single-energy x-ray diffraction pattern [11]. We can estimate the relative contributions of the holographic process and the Patterson process, taking account of the electron scattering factor of the Si atom [shown in Fig. 1(c)]. For the specific scattering configuration shown in Figs. 1(a) and 1(b), the singly scattered wave amplitude f_C can be crudely estimated to be 4 times larger than that of the doubly scattered wave f_B. A similar argument also holds even if the emitter atom in Fig. 1(a) is an adsorbed heavy atom. Thus we may expect that the single scattering process contributes largely to the modulation of the $I(E)$ curves, and we propose that the 3D atomic images can be obtained from direct Patterson inversion of multiple-energy LEED patterns. Such a direct inversion scheme is conceptually different from the holographic scheme. Using Si(113)-(3 × 2) and Si(111)-(7 × 7) surfaces as examples, we can obtain high quality 3D atomic images

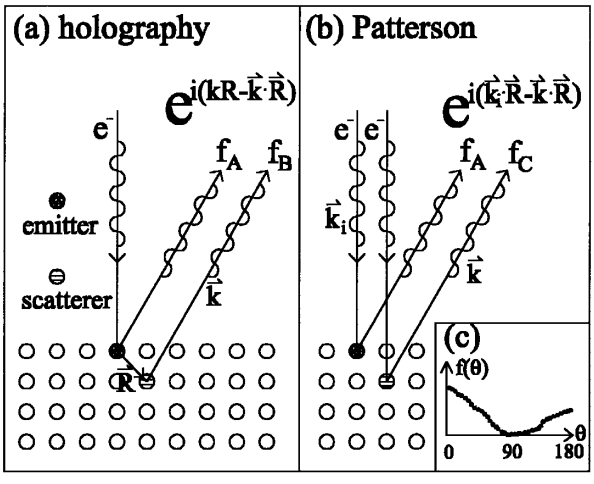

FIG. 1. Schematic diagrams of (a) the holographic diffraction process, (b) the Patterson single scattering process, and (c) the electron scattering factor $f(\theta)$ of the Si atom as a function of the scattering angle θ (in degrees). The energy of the electron is 100 eV.

 0031-9007/99/83(13)/2580(4)$15.00

of surface and bulk atoms with direct Patterson inversion of LEED-$I(E)$ curves.

In this Letter, the integral-energy phase-summing method (IEPSM) was applied to the measured LEED-$I(E)$ curves for image reconstruction [5,6,12]. The formula for holographic inversion is

$$\sum_{\mathbf{k}} \int g(k)\chi(\mathbf{k})e^{-i(kR-\mathbf{k}\cdot\mathbf{R})}k^2\,dk\,, \qquad (1)$$

where $\mathbf{k}$ is the out-going electron wave vector, $\mathbf{R}$ is the relative position vector of the atomic pair, $g(k)$ is the window function for the transform, $\chi(\mathbf{k}) = [I(\mathbf{k}) - I_0(\mathbf{k})]/I_0(\mathbf{k})$ is the normalized intensity modulation in which $I_0(k)$ is a low-order polynomial fit of $I(\mathbf{k})$ as an intensity background, and then sum over all diffraction directions. The inversion formula (1) works well for photoelectron holography, diffused LEED holography, and Kikuchi electron holography (KEH).

The above formula for holographic inversion can be generalized to Patterson inversion, that is

$$\sum_{\mathbf{k}} \int g(k)\chi(\mathbf{k})e^{-i(\mathbf{k}_i\cdot\mathbf{R}-\mathbf{k}\cdot\mathbf{R})}k^2\,dk\,, \qquad (2)$$

where $\mathbf{k}_i$ is the incidence electron wave vector. The phase factor in the holographic inversion (1) accounts for the phase difference introduced by the path difference between the reference wave (emitted from the emitter) and the scattered wave from an atom (the scatterer) nearby the emitter. The phase factor in Eq. (1) is independent of the incident electron beam. However, the phase factor in the Patterson inversion (2) is to account for the interference effect of the singly scattered waves of the incident electron beam. The results inverted by the holographic inversion formula (1) or the Patterson inversion formula (2) are the 3D atomic images relative to the emitter or the Patterson origin in the latter case.

The diffraction direction $\mathbf{k}$ is limited to the discrete LEED spots determined by the translation symmetry of the sample. The integer-order LEED spots are mostly due to the electron scattering of atoms with 1×1 substrate translation symmetry, if the surface reconstruction in not too deep, while the fractional-order spots must involve at least one surface atom with $n \times m$ superstructure translation symmetry. Thus the structural information contained in integer-order and fractional-order beams is different. In our experiment, a rearview LEED optics is used to display the LEED patterns, which are then recorded by a charge coupled device camera. The energy range is from 70 to 250 eV. The reconstructed atomic images are not sensitive to the inner potential chosen for inversion. We have performed the Patterson and holographic inversion of integer-order and fractional-order LEED-$I(E)$ curves of normal incident configuration with IEPSM.

Shown in Fig. 2 is the puckering tetramer Ranke's structure model of the 3×2 surface [13]. In Fig. 3, we show the reconstructed atomic images of integer-order beams of the 3×2 surface with the Patterson inversion scheme. Note that there is no huge peak at the Patterson origin, which is the consequence of the subtraction of a smooth background before the Fourier transform is performed. This is one of the reasons that Patterson LEED is successful now. Another reason is the large set of experimental data used for inversion. The bright spots indicate the relative position vectors of atomic pairs that exist in the sample. The atomic images fit quite well (within 0.2 Å) with the relative positions between the bulk atoms. While for the atomic images obtained by holographic inversion, the positions of image spots deviate from the bulk values by an amount of up to $\sim$1.0 Å, and they could not be assigned to the atomic pairs in the bulk, except for the atomic images near-z direction. Thus we can conclude that the single scattering process in the bulk region contributes mostly to the intensity modulation in the LEED-$I(E)$ curves of integer-order beams. The differences between the resulted images of holographic and Patterson inversion schemes can be explained by comparing the phase factors in formulas (1) and (2). The two phase factors differ by a term $\exp[i(kR - \mathbf{k}_i \cdot \mathbf{R})]$. For normal incidence configuration, where $\mathbf{k}_i = (0, 0, -k)$ and $\mathbf{R} = (x, y, z)$, this term results in $\exp[ik(R + z)]$. Thus, for the atomic pairs that the scatterer is right beneath the emitter, i.e., $z = -R$, there is no difference in phase factors for both Patterson and holographic inversions, and the two inversions will yield the same results. While for the atomic pairs not in strictly backward direction ($-z$ direction), as position vector $\mathbf{R}$ of the atomic pair points gradually away from the incident direction, the difference of two inversion schemes will come out and become larger.

Shown in Fig. 4 is the reconstructed atomic images of $I(E)$ curves of fractional-order beams of the 3×2 surface by using the Patterson inversion scheme. Besides

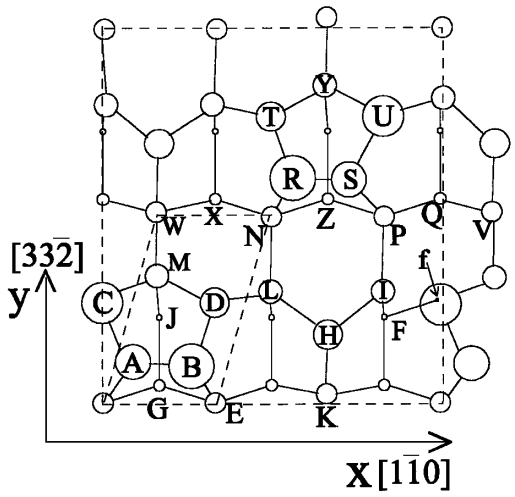

FIG. 2. Puckering tetramer Ranke's model of Si(113)-(3×2) surface. The atom symbols are bigger for the atoms in the outer atomic layer. The dashed lines outline the 1×1 and 3×2 unit cells.

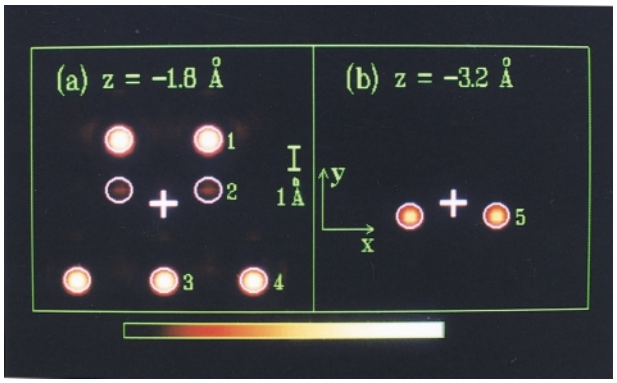

FIG. 3 (color). Patterson inverted images of integer-order LEED spots of Si(113)-(3 × 2) surface of normal incident configuration (a), (b): Top views of atomic images of z-plane cuts for (a) $z = -1.8$ Å, and (b) $z = -3.2$ Å, respectively. The cross symbol marks the projection of the origin on the z plane. The center of the circle marks the correct relative position of the atomic pair.

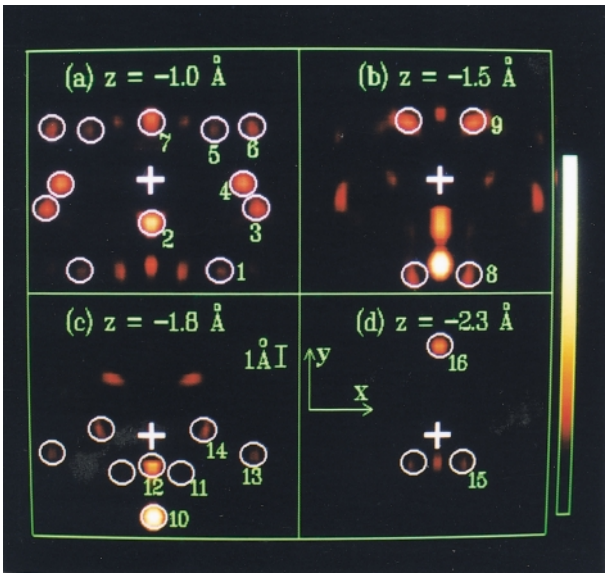

FIG. 4 (color). Patterson inverted images of fractional order spots of the Si(113)-(3 × 2) surface. (a)–(d) are the top views of atomic images of four z-plane cuts of -1.0, -1.5, -1.8, and -2.3 Å, respectively. The center of the circle marks the correct relative position of the atomic pair.

the atomic images that can get proper correspondence to the bulk structure, many atomic images reveal the characteristics of puckering tetramer Ranke's model of the 3 × 2 surface. For example, image spots 11 and 15 could be understood as the images as viewing from S to P and from B to E (from the buckling dimer to the underlying bulk atom, in Fig. 2), respectively. In Table I, we list the reconstructed atomic images, the corresponding atomic pairs in the puckering tetramer Ranke's model, and the expected image positions that are obtained from the *ab initio* total energy calculation conducted by Wei [14]. We also performed holographic inversion of the fractional order $I(E)$ curves, and the resulted atomic images could not get proper assignment to the existing structure models.

We also performed the same studies on a 7 × 7 surface. Patterson inversion of integer-order beams results in the bulk structural information, as could be expected, while Patterson inversion of fractional-order beams indeed contains the surface structure information. Shown in Fig. 5 is the reconstructed atomic images of the fractional-order $(\frac{1}{7}, 0)$ beam set of $I(E)$ curves [i.e., $(\frac{1}{7}, 0) \pm h\mathbf{G}_1 \pm k\mathbf{G}_2$ and symmetry-equivalent beams, where $\mathbf{G}_1, \mathbf{G}_2$ are 1×1 reciprocal lattice vectors and h, k are integers]. The reconstructed atomic image spots are almost sixfold symmetric, except the 0.2 Å difference in the z coordinate between spot 1 and 2 (or 3, 4). This observation is consistent with certain building blocks in the fault and unfault region of the dimer-adatom-stacking-fault model of the 7 × 7 surface [15]. Other beam sets also contain the structural information of the surface building blocks.

Using IEPSM for inversion, twenty integral beams are sufficient to produce the images of the bulk atomic pairs with noise level less than 15%. Although the sampling density of the LEED pattern will result in the repeated points in **R** space, caused by the discrete sampling theorem of Fourier transform, these repeated points would be easily recognized by its repetition nature, and would not perplex the interpretation of the reconstructed images.

The difference between the Patterson and the holographic ideas is clearly seen in Fig. 1. In the holographic process, a local source of emitted electron, which has lost its phase coherence, is needed. Thus, the holographic inversion should work for Kikuchi electron and photoelectron. Whereas in the Patterson (LEED) process, the

TABLE I. The positions of image spots of Si(113)-(3 × 2) surface by Patterson inversion. Also listed are the corresponding atomic pairs and the theoretical relative positions of the atomic pairs in puckering tetramer Ranke's model (Fig. 2). The image spots are numbered in Fig. 4.

Image spots	Reconstructed spot coordinate (Å)	Atomic pair	Theoretical atomic images (Å)
1	(2.9, −4.0, −1.2)	*S-L*	(2.9, −3.9, −1.0)
2	(0.0, −2.0, −1.0)	*H-K*	(0, −2.2, −1.3)
3	(4.4, −0.9, −1.6)	*S-V*	(4.6, −1.0, −1.4)
4	(3.8, 0.0, −1.0)	*C-D*	(3.7, 0.3, −0.5)
5	(2.9, 2.0, −1.0)	*R-U*	(2.8, 1.8, −0.5)
6	(4.7, 2.1, −1.5)	*A-L*	(4.9, 2.4, −1.1)
7	(0.0, 2.7, −1.0)	*M-W*	(0, 0, 2.3, −0.5)
8	(1.1, −4.1, −1.5)	*S-I*	(0.7, −3.7, −1.5)
9	(1.4, 2.8, −1.7)	*R-Y*	(1.2, 3.2, −1.4)
10	(0.0, −3.8, −1.7)	*M-G*	(0.0, −3.9, −1.8)
11	(1.0, −1.7, −1.7)	*S-P*	(0.8, −1.5, −1.4)
12	(0.0, −1.3, −1.8)	*M-J*	(0.0, −1.5, −2.0)
13	(4.4, −1.0, −2.0)	*B-K*	(4.7, −0.7, −1.9)
14	(2.0, 0.1, −1.6)	*W-X*	(1.9, 0.1, −1.2)
15	(0.9, −1.3, −2.4)	*B-E*	(0.7, −1.4, −2.1)
16	(0, 0, 4.2, −2.6)	*H-Z*	(0.0, 4.4, −2.5)

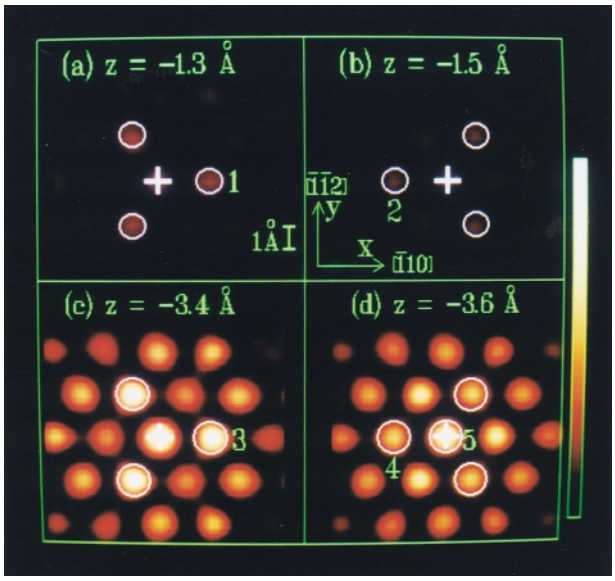

FIG. 5 (color). Patterson inverted atomic images of fractional order $(\frac{1}{7}, 0)$ beam set of Si(111)-(7 × 7) LEED spots (see text). (a)–(d): Top views of atomic images of four z-plane cuts of −1.3, −1.5, −3.4, and −3.6 Å, respectively.

externally incident electrons are diffracted in a phase coherent way. Also for LEED, the single elastic scattering dominates over the various kinds of multiple scattering. Thus Patterson inversion is needed to reconstruct the multiple-energy LEED patterns. In both cases, the IEPSM must be used to eliminate the multiple scattering effects and to reconstruct the atomic images with Eqs. (1) and (2), respectively.

In conclusion, the Patterson inversion scheme works very well for LEED-$I(E)$ experiments, and the surface sensitivity is guaranteed by using fractional-order beams, in which the scattering process involves at least one of the surface atoms, for inversion. Using Si(113)-(3 × 2) and Si(111)-(7 × 7) surfaces as examples, clear atomic images, with a resolution of 0.5 Å, are obtained for the normal incidence configuration. The relative positions of the surface atom to the bulk atom are easily imaged, while the surface building blocks can be imaged by using glancing KEH [16,17]. It will be possible that surface structure determination, by using direct inversion of LEED-$I(E)$ curves as well as glancing Kikuchi patterns, in conjunction with scanning tunneling microscopy, becomes a routine work in an ordinary laboratory. Only after the surface structure that is close to the true structure has been determined, could the conventional refinement method, e.g., LEED dynamical calculation, be applied for the final determination of the surface structure.

This work was supported by the National Science Council, Republic of China, under Grant No. NSC-87-2613-M-007-005.

[1] M. A. Van Hove, W. H. Weinberg, and C.-M. Chan, *Low-Energy Electron Diffraction* (Springer-Verlag, Berlin, Heidelberg, 1986).
[2] David L. Adams and Uzi Landman, Phys. Rev. B **15**, 3775 (1977).
[3] M. G. Lagally, T. C. Ngoc, and M. B. Webb, Phys. Rev. Lett. **26**, 1557 (1971).
[4] J. J. Barton, Phys. Rev. Lett. **61**, 1356 (1888), and references therein.
[5] S. Y. Tong, Hua Li, and H. Huang, Phys. Rev. Lett. **67**, 3102 (1991).
[6] J. J. Barton, Phys. Rev. Lett. **67**, 3106 (1991).
[7] M. A. Mendez, C. Glük, and K. Heinz, J. Phys. Condens. Matter **4**, 999 (1992).
[8] P. Hu and D. A. King, Nature (London) **360**, 656 (1992).
[9] S. Y. Tong, H. Huang, and X. Q. Guo, Phys. Rev. Lett. **69**, 3654 (1992).
[10] K. Reuter *et al.*, Phys. Rev. Lett. **79**, 4818 (1997).
[11] M. J. Buerger, *Vector Space and Its Application in Crystal-Structure Investigation* (Wiley, New York, 1959).
[12] C. M. Wei and S. Y. Tong, Surf. Sci. **274**, L577 (1992).
[13] J. Wang, A. P. Horsfield, S. G. Pettifor, and M. C. Payne, Phys. Rev. B **54**, 13 774 (1996).
[14] C. M. Wei (unpublished).
[15] S. Y. Tong *et al.*, J. Vac. Sci. Technol. A **6**, 615 (1988).
[16] C. M. Wei, I. H. Hong, and Y. C. Chou, Surf. Rev. Lett. **1**, 335 (1994).
[17] I. H. Hong *et al.*, Phys. Rev. B **54**, 4762 (1996).